

Application of Vector Spherical Harmonics to the Magnetisation of Mars' Crust

David Gubbins^{1,2}, Yi Jiang², Simon E. Williams³, Keke Zhang²

¹School of Earth and Environment, University of Leeds, UK

²State Key Laboratory of Lunar and Planetary Science, Macau University of Science and Technology,
Macau

³State Key Laboratory of Continental Dynamics, Department of Geology, Northwest University, Xi'an,
China

Key Points:

- Vector spherical harmonic analysis can help elucidate magnetic structures in Mars' crust
- Secondary magnetisation in a uniform shell produces a magnetic anomaly that reflects the original dynamo field
- Absence of anomalies at large impact craters cannot be explained by simply excavating magnetised crust

Corresponding author: D. Gubbins, gubbins@earth.leeds.ac.uk

Abstract

Mars has a magnetic field originating in its strongly magnetised crust that holds clues to the planet’s interior. We apply vector spherical harmonic decomposition to simple candidate magnetic structures to separate the parts responsible for the anomalies from those that remain invisible. A uniform magnetic layer produces no anomalies: spatial variations are essential although secondary magnetisation does produce a weak field that might reflect the primordial dynamo field. A hemispheric layer produces anomalies confined to the equator rather than the observed hemispheric difference. A uniformly magnetised crust with variable thickness determined from gravity and topography produces a crustal field with large anomalies at the major impact crater sites that are not observed. These anomalies are not present if the magnetic layer lies deeper than the crater floor. We conclude that decomposing magnetisations in this way is a useful tool in the interpretation of Martian magnetic anomalies.

Plain Language Summary

Four billion years ago Mars had a magnetic field generated by a dynamo operating in its liquid core, as Earth has today. It cooled faster than Earth and dynamo action ceased but not before it had magnetised the planet’s crust. This study is made topical by the arrival of the Chinese rover Zhurong, which is capable of carrying out a ground magnetic survey. The lander InSight recorded a magnetic field some ten times stronger than expected from measurements made by satellite in orbit. Here we use a relatively new technique to separate proposed magnetic structures into their “invisible” and “visible” parts. We show this while the magnetic field is stronger in the Southern Hemisphere than the North, this does not imply one hemisphere is more strongly magnetised than the other. Strong ground measurements can be explained by a strongly magnetised, invisible, shell that has been broken up into smaller, visible, fragments. Larger impact craters have no magnetic anomaly, an observation often attributed to removal of the original magnetised material; we show the anomaly remains if the surrounding crust is strongly magnetised and propose the source of the anomalies lies deeper than the bottom of these craters.

1 Introduction

Determining magnetisation from observations of the crustal magnetic field is difficult because a wide variety of magnetised bodies do not have an observable field. This problem is particularly acute when the magnetisation is remanent, as on Mars, rather than induced, as on much of Earth’s continents, because all 3 components of the vector magnetisation must be found rather than just the scalar susceptibility. Most interpretation is therefore done by forward modelling using a candidate distribution of magnetisation. Decomposition into vector spherical harmonics (VSH) separates the part of the magnetisation responsible for the observed field, the “visible” part, from the part that produces no magnetic field, the “invisible” part (Gubbins et al., 2011). This is useful because knowing the invisible part can direct further study using different data, such as gravity, geology, and topography. In this preliminary study we explore the value of VSH decomposition of models of Mars’ crust.

Mars’ remanent magnetisation has the same hemispheric dichotomy as the gravity field and topography: lowland plains in the Northern Hemisphere have weak magnetic fields whereas the mountains of the Southern Hemisphere have strong magnetic fields. The dichotomy is the oldest geology (Watters et al., 2007; Bottke & Andrews-Hanna, 2017), thought to have formed when a dynamo was active in the core of Mars (Mittelholz et al., 2020). Younger craters (e.g. Hellas, Isidis, Argyre) are thought to have formed after the dynamo ceased to operate at around 4.1 Ga (Lillis et al., 2008) because they lack magnetic anomalies; anomalies of even younger craters (e.g. Apollonius Pateras, Lucius

Planum) point to an active dynamo as late as 3.8 Ga (Hood et al., 2010; Mittelholz et al., 2020). Either there was a gap in dynamo activity around 4.1-3.8 Ga or craters have been demagnetised (Mittelholz et al., 2020).

Satellite missions to Mars have resulted in several orbital models of the global magnetic field, reviewed recently by (Smrekar et al., 2018). Here we use the most recent one of Langlais et al. (2019), which has resolution around 150 km. There is a single ground measurement, made by the lander InSight, which is some ten times that predicted by the orbital model (Johnson et al., 2020) and promise of further ground data in the near future from the Chinese rover Zhurong, which carries a magnetometer that could produce a small-scale survey.

Mars' crustal remanence is some ten times stronger than Earth's. It depends on the strength, morphology and timing of the primordial dynamo field, the magnetic minerals in the crust, and the thickness of the magnetised layer. Most studies start from a shell that becomes magnetised as the planet cooled early in its history, which is altered by subsequent activity [e.g. Milbury and Schubert (2010)]. Arkani-Hamed (2003, 2005) considered *secondary magnetisation* of a deeper layer that cooled below the Curie temperature after dynamo action ceased and was magnetised by the overlying magnetic layer. The depth of the magnetic layer is estimated at 30–72 km from spectra (Voorhies, 2008; Lewis & Simons, 2012; Gong & Wiczeorek, 2021), with an average of 50 km, close to the crustal thickness estimated from gravity and topography (Wiczeorek et al., 2019). Solomon et al. (2005) suggest the magnetic anomalies are associated with variations in crustal thickness.

Two theories of the origin of the dichotomy are debated: degree-1 mantle convection, which formed the northern plains and southern highlands (Zhong & Zuber, 2001; Nimmo & Gilmore, 2001; Ke & Solomatov, 2006) and giant impact or impacts hitting what is now the Northern Hemisphere (Frey & Schultz, 1988; Marinova et al., 2008; Andrews-Hanna et al., 2008; Bottke & Andrews-Hanna, 2017). Most authors have assumed a dipolar primordial dynamo field and there are many estimates of primordial paleopoles (Thomas et al., 2018). Stanley et al. (2008) explain the strong southern hemisphere magnetic fields with a hemispheric dynamo, which has magnetic field confined to one hemisphere. Degree-1 mantle convection or a giant impact could produce strong heat flux variations on the core-mantle boundary, inducing downwelling in the core. This concentrates magnetic field lines over the downwelling, a mechanism used to explain the concentration of Earth's magnetic field on the longitudes of the subduction zones of the Pacific rim (Bloxxham & Gubbins, 1987).

The major magnetic features to be explained are the absence of strong anomalies in the northern lowlands, major impact basins of Hellas, Isidis, and Argyre, and part of the Tharsis bulge. These absences have been attributed to many different causes, including variation in crustal thickness, thermal demagnetisation, burial by later lavas erupted after dynamo action ceased, impact demagnetisation by excavation, and hydrothermal alteration (Solomon et al., 2005; Lillis et al., 2008, 2009; Morschhauser et al., 2018; Mittelholz et al., 2020). Thus a weak magnetic field region is normally taken to mean the crust beneath is weakly magnetised or thin, as in the northern lowlands; likewise, strong magnetic anomalies in the southern highlands are taken to mean strongly magnetised or thick crust. However, the relationship between magnetisation and magnetic field is not so simple: here we challenge this simplistic interpretation.

Our forward modelling approach starts from a simple geologically plausible model of magnetisation that is decomposed into VSH to determine the extent of the invisible part. The geological foundation is then progressively refined to improve the fit to the observations. In this preliminary survey we use VSH decomposition to study 3 simple possible scenarios: a uniform crust that is strongly magnetised everywhere, a new analysis of Arkani-Hamed's secondary magnetisation, and anomalies caused by a uniformly mag-

netised crust of variable thickness. It follows comparable studies for the Earth (Masterton et al., 2012; Williams & Gubbins, 2019).

2 Method

The VSH are simple combinations of scalar spherical harmonics

$$\mathbf{Y}_{n,n+1}^m = \frac{r^{n+2}}{\sqrt{(n+1)(2n+1)}} \nabla \left[\frac{1}{r^{n+1}} Y_l^m(\theta, \phi) \right] \quad (1)$$

$$\mathbf{Y}_{n,n}^m = -\frac{i}{\sqrt{n(n+1)}} \mathbf{r} \times \nabla Y_n^m(\theta, \phi) \quad (2)$$

$$\mathbf{Y}_{n,n-1}^m = \frac{1}{r^{n-1} \sqrt{n(2n+1)}} \nabla [r^n Y_n^m(\theta, \phi)], \quad (3)$$

where (r, θ, ϕ) are spherical coordinates and Y_n^m is a complex mean-normalised scalar spherical harmonic of degree and order n, m . They are complete and orthogonal when integrated over the sphere. The appearance of r in (1)–(3) is illusory because it differentiates out. The VSH are written in this way to bring out the connection with the 3 types of solution of Laplace’s equation: the potential field finite at infinity, $\mathbf{Y}_{n,n+1}^m$, the one finite at the origin, $\mathbf{Y}_{n,n-1}^m$, and the toroidal one, $\mathbf{Y}_{n,n}^m$, that has an associated radial electric current.

In this paper we deal only with the vertically integrated magnetisation (VIM) and assume magnetisation is confined to a surface shell that is thin compared to the radius of the planet. We expand the VIM in VSH:

$$\bar{\mathbf{M}}(\theta, \phi) = \sum_{n,m} [E_l^m \mathbf{Y}_{n,n+1}^m(\theta, \phi) + I_n^m \mathbf{Y}_{n,n-1}^m(\theta, \phi) + T_n^m \mathbf{Y}_{n,n}^m(\theta, \phi)] = \mathcal{E} + \mathcal{I} + \mathcal{T}, \quad (4)$$

where E_l^m, I_l^m, T_l^m are complex coefficients. Orthogonality gives

$$E_n^m = \frac{1}{4\pi} \oint \bar{\mathbf{M}} \cdot (\mathbf{Y}_{n,n+1}^m)^* d\Omega \quad (5)$$

$$I_n^m = \frac{1}{4\pi} \oint \bar{\mathbf{M}} \cdot (\mathbf{Y}_{n,n-1}^m)^* d\Omega \quad (6)$$

$$T_n^m = \frac{1}{4\pi} \oint \bar{\mathbf{M}} \cdot (\mathbf{Y}_{n,n}^m)^* d\Omega, \quad (7)$$

where $*$ denotes the complex conjugate.

The associated magnetic fields in the non-magnetic, insulating external and internal regions are found by substituting into the usual Poisson integral. This shows that the $\{\mathbf{Y}_{n,n-1}^m\}$ produce a potential outside the sphere but none inside it, the $\{\mathbf{Y}_{n,n+1}^m\}$ inside the sphere but none outside it, and the $\{\mathbf{Y}_{n,n}^m\}$ no potential field at all because the associated radial electric current cannot flow in the insulator. Furthermore, the $\mathbf{Y}_{n,n-1}^m$ coefficients, $\{I_n^m\}$, are related to the usual Gauss coefficients:

$$g_n^m = \frac{\mu_0}{R_{\odot}} \sqrt{n\epsilon_m} \Re(I_n^m) \quad (8)$$

$$h_n^m = -\frac{\mu_0}{R_{\odot}} \sqrt{n\epsilon_m} \Im(I_n^m), \quad (9)$$

where \Re and \Im denote the real and imaginary parts. The $\{E_n^m\}$ are related to the coefficients describing a potential field inside the shell:

$$r_n^m = \frac{\mu_0}{R_{\odot}} \sqrt{(n+1)\epsilon_m} \Re(E_n^m) \quad (10)$$

$$s_n^m = -\frac{\mu_0}{R_{\odot}} \sqrt{(n+1)\epsilon_m} \Im(E_n^m), \quad (11)$$

where R_{\odot} is Mars' radius, μ_0 is the permeability of free space, and $\epsilon_m = 2$ if $m = 0$ and 1 otherwise. The $\{I_n^m\}$ therefore describe the visible part of the magnetisation, the E_n^m and T_n^m the invisible part, i.e. the complete null space of the inverse problem of VIM from magnetic field data. Full details of the method are in Gubbins et al. (2011).

Consider a uniform shell magnetised by an internal potential field, such as an initially hot Martian crust cooling from top down bathed in the magnetic field of an early dynamo. The magnetising field is of internal origin and therefore \mathcal{E} . The VIM, whether induced or remanent, is a constant multiplied by the field and therefore also \mathcal{E} with magnetic anomalies confined within the shell: nothing observable. Similarly, an external magnetising field, such as produced by an upper layer that has already cooled below the Curie temperature, will be \mathcal{I} and magnetise the deeper layer to give magnetic anomalies outside the shell but not inside. These statements apply whatever the configuration of the magnetising field, they are not restricted to a dipole.

3 A Uniform Shell With Secondary Magnetisation

3.1 Strong VIM beneath weak magnetic anomalies

If Mars began with a uniform shell cooling from above and magnetised dynamo-generated field \mathbf{B} its VIM would be

$$\bar{\mathbf{M}} = \Xi d \mathbf{B} / \mu_0, \quad (12)$$

where the constant d is the thickness of the magnetised layer and the magnetising constant $\Xi = K\chi/(1 + \chi)$ can be estimated from the Koenigsberger ratio K and susceptibility χ . For dipole \mathbf{B} the magnetisation is described by coefficients given by: $E_1^0 = -(\Xi d / \mu_0) \sqrt{2} g_1^0$ and $E_1^1 = -(\Xi d / \mu_0) (g_1^1 - i h_1^1)$. The strength of VIM is determined by a single scalar, the product of the dipole moment and Ξd , which can be adjusted within reasonable bounds.

This basic VIM must be altered if it is to fit the present-day data. To do this we add an \mathcal{I} component based on the Gauss coefficients of Langlais et al. (2019) using equations (8) and (9). The resulting VIM fits the data exactly and contains an arbitrarily strong background magnetisation. Although the uniform shell does not produce any external magnetic field it does change the orientation and strength of the VIM locally. In particular it affects the VIM at landing sites and will partly determine the large anomalies not seen at satellite altitude.

Three examples of the radial component of VIM are shown in Figure 1 for 3 dipole orientations: axial, equatorial and one taken from previous estimates of Mars' paleopole (Milbury & Schubert, 2010). We have chosen $K = 1$, $\chi = 0.2$, $d = 40$ km, and $G = \sqrt{g_1^{02} + g_1^{12} + h_1^{12}} = 30,000$ nT: reasonable values for magnetic minerals, a commonly quoted thickness for Mars' magnetised crust, and an Earth-like dipole field. These choices make the strength of magnetisation of the uniform shell comparable with that required to satisfy the magnetic field model. In Table 1 we give the magnetic vectors at the landing sites of InSight and Zhurong. The differences in magnetic vectors caused by the uniform shell and different dipole orientations is clear.

3.2 Secondary Magnetism

Arkani-Hamed (2003) considered cooling of Mars' crust beyond the duration of dynamo action, giving 2 shells, the upper one magnetised by the dynamo and the lower one by the magnetic field of the upper one. Suppose for simplicity the outer shell, thickness d_u , was magnetised by an axial dipole; its VIM is described by the single VSH coefficient $E_1^0 = (\Xi d_u / \mu_0) \sqrt{2} g_1^0$, which produces a field inside the shell with coefficient

$$r_1^0 = \sqrt{2} \mu_0 E_1^0 / R_{\odot} = 2 \Xi g_1^0 d_u / R_{\odot}.$$

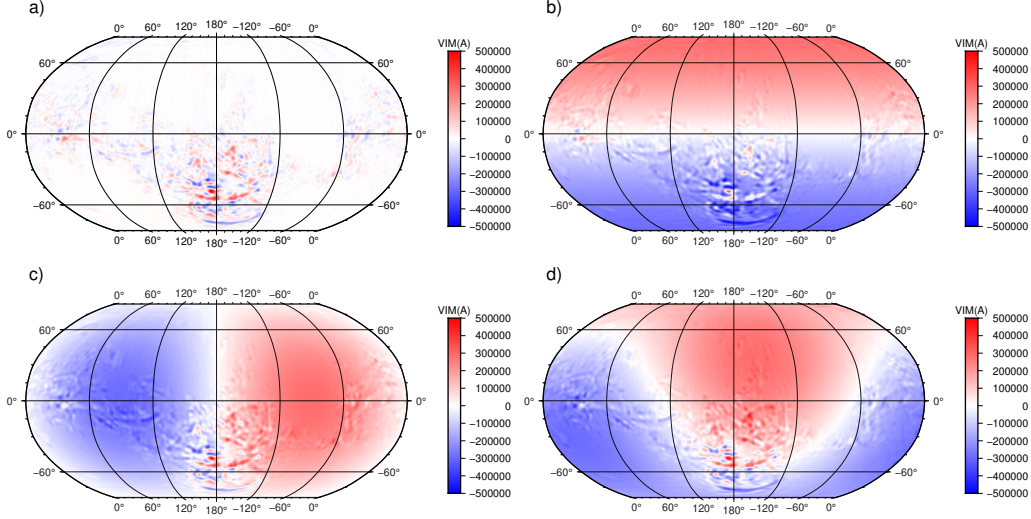


Figure 1. Radial components of VIM by different dipoles. a: \mathcal{I} “visible” part based on the satellite field using (8) and (9); b: addition of a uniform shell magnetised by an internal axial dipole; c: same for an equatorial dipole with paleopole 0°N, 270°E; d: for a dipole with paleopole 34°N, 202°E.

The internal shell, now grown by continued cooling to a thickness d_1 , is magnetised by the external field with VIM described by a single VSH coefficient $I_1^0 = \Xi d_1 / \mu_0 r_1^0 = 2\Xi^2 d_u d_1 / \mu_0 R_{\mathcal{J}}$. The secondary magnetisation of the inner shell produces an external field with Gauss coefficient

$$j_1^0 = \mu_0 I_1^0 / R_{\mathcal{J}} = 2\Xi^2 (d_u / R_{\mathcal{J}}) (d_1 / R_{\mathcal{J}}) g_1^0. \quad (13)$$

This external field is a reflection of the primordial dynamo field reduced by the factor $\Xi^2 (d_u / R_{\mathcal{J}}) (d_1 / R_{\mathcal{J}})$. Taking the previous value for g_1^0 , Ξ , and $d_u = d_1 = 20$ km gives $j_1^0 \approx 1$ nT, the same order of magnitude as the orbital model’s $n = 1$ terms but much smaller than the high degree terms. The similarity in orders of magnitude make secondary magnetisation an interesting possible contributor but, in agreement with Arkani-Hamed (2005), we find it too small to explain the small-scale anomalies.

The same analysis applies to a dynamo field of any configuration. In future, if the crustal structure can be tied down sufficiently accurately, secondary magnetisation offers an interesting window on Mars’ original dynamo field.

4 A Magnetised Shell of Variable Thickness

We now explore to what extent the magnetic anomalies can be explained by variable crustal thickness. The hemispheric dichotomy suggests a thin layer in the Northern Hemisphere and a thick layer in the Southern Hemisphere. The resulting magnetisation by any primordial field is a substantial \mathcal{E} part resulting from a uniform layer with Northern Hemisphere thickness plus an extra Southern Hemisphere layer also dominated by \mathcal{E} except on the boundary because it is uniform within the hemisphere. The resulting magnetic field is concentrated around the equator irrespective of the primordial magnetising field. More details are in the Supplementary Information, see Figures S1-3.

We next assume a crust with uniform magnetic properties but variable thickness $d(\theta, \phi)$ derived from topography and gravity using the methods described in Wicczorek et al. (2019). Figure 2 shows the initial thickness assuming a uniform crustal density 2.9 kg/cm³, mantle density 3.4 kg/cm³, imposed 40 km thickness at the InSight landing site,

Lander	InSight			Zhurong		
	Mag	Dip	Az	Mag	Dip	Az
\mathbf{B} nT	309.91	-73°	135°	80.65	47°	55°
$\mathbf{M}(\mathcal{I})$ kA	17.2	-57°	-61°	5.78	55°	-157°
$\mathbf{M}(\text{axi})$ kA	159	-14°	-177°	195	-41°	0.03°
$\mathbf{M}(\text{equ})$ kA	241	60°	-92°	289	73°	-140°
$\mathbf{M}(\text{gen})$ kA	229	51°	-128°	204	51°	-160°

Table 1. Magnetic fields and magnetisations at the sites of 2 landers on Mars. Their locations are: InSight (4.5°N,135.6°E), Zhurong (25.1°N,109.9°E). \mathbf{B} denotes the magnetic field computed from the satellite model of Langlais et al. (2019). $\mathbf{M}(\mathcal{I})$ the vector VIM in Amps computed by converting the Gauss coefficients of the orbital model to I_n^m using equations (8) and (9). The last 3 lines are VIMs after addition of a uniform shell magnetised by a dipolar dynamo field with axial, equatorial, and general paleopoles as described in the text. Note the dominance of the magnetisation of the uniform shell, an order of magnitude larger than the \mathcal{I} part. This is because of the dominance of the \mathcal{E} part from magnetisation by an internal field. The same applies to the Earth (Masterton et al., 2012).

and maximum spherical harmonic degree 90. The VIM is, from (12), $\bar{\mathbf{M}}(\theta, \phi) = [\Xi d(\theta, \phi)/\mu_0] \mathbf{B}(\theta, \phi)$ with magnetic parameters modified to fit the average magnitude of the orbital model: $K = 3$ and $\chi = 0.5$, and $G = -30,000$ nT.. We use the same 3 primordial paleopoles

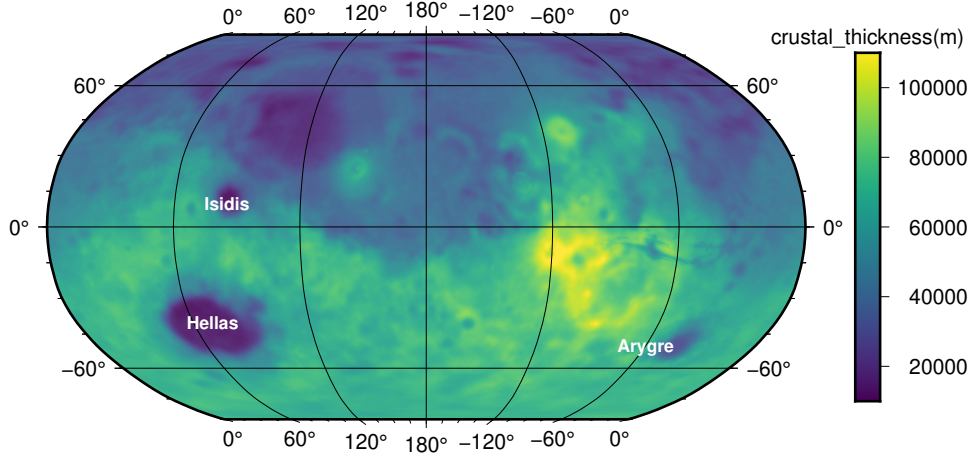


Figure 2. Crustal thickness for Mars based on inversion of topography and gravity data (Wieczorek et al., 2019).

as before.

Each VIM is decomposed into VSH as illustrated in Figure 3. Only the radial component is shown, for which the toroidal component is zero. Note that the \mathcal{E} part on the left reflects the dipole orientation and some of the variations in crustal thickness, most noticeably the Hellas basin; it is some 10 times larger than \mathcal{I} : the relative sizes (RMS) of the total VIMs are $\mathcal{E} : \mathcal{T} : \mathcal{I} = 81:9:10$. \mathcal{E} dominates because the crustal thickness is, to a first approximation, a uniform shell and it is magnetised by an internal field. The

222

\mathcal{I} part is mainly determined by variations in crustal thickness rather than dipole orientation.

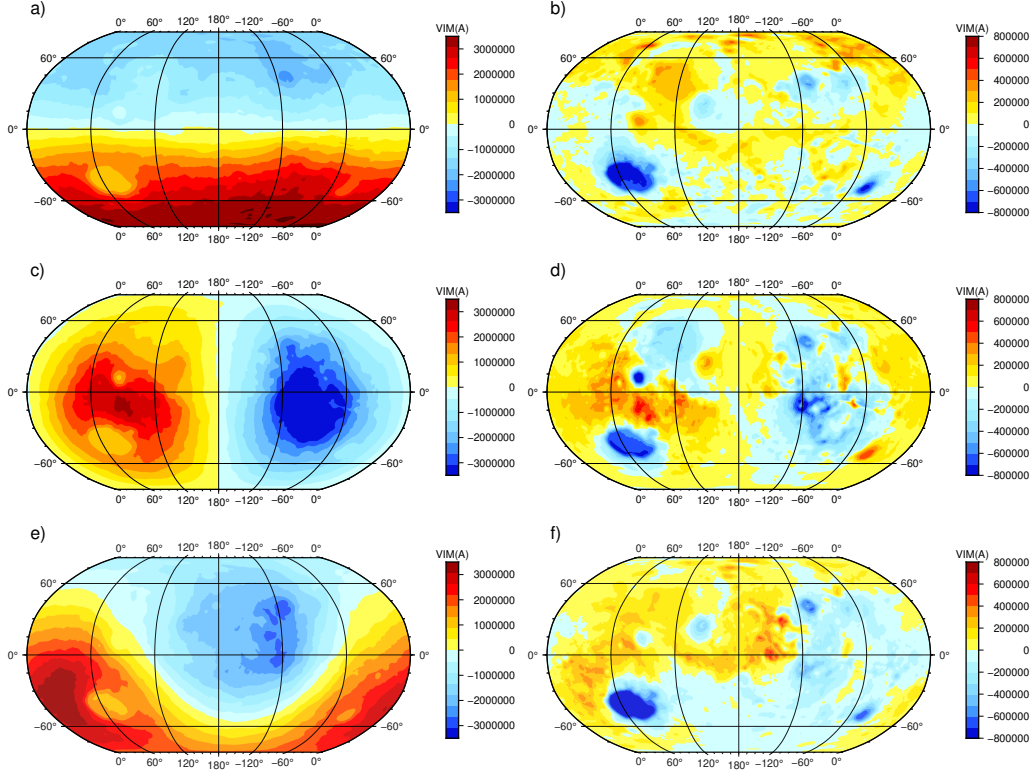


Figure 3. VSH decomposition of the radial component of VIM for 3 paleopoles. Columns are \mathcal{E} (left) and \mathcal{I} (right); rows are for axial, equatorial ($0^\circ\text{N}, 270^\circ\text{E}$), and general ($34^\circ\text{N}, 202^\circ\text{E}$) paleopoles. Radial component for \mathcal{T} is zero.

223

224 Radial magnetic fields are shown in Figure 4. Like the \mathcal{I} part, the field patterns
 225 are relatively insensitive to dipole orientation. The wavelengths are similar to the orbital
 226 model but there are large discrepancies, most noticeably the anomalies over major im-
 227 pact craters Hellas, Isidis, and Argyre. The crustal models all produce crater anomalies
 228 that are wholly absent from the orbital model. Hellas has the largest anomaly; it lies in
 229 a region of thick (>60 km) crust and has a sharp step around its edge that produces the
 230 more intense ring on the boundary (Figures 4, 5). Isidis lies in a region of thinner crust
 231 and the anomaly is not so prominent (Figure S5). Magnetic anomalies are more subdued
 232 or absent along more gradual gradients in crustal thickness such as the dichotomy bound-
 233 ary and the margins of Utopia Planitia. This suggests the sharp jumps in VIM near the
 234 periphery of the boundaries are responsible for at least part of the anomalies. Absence
 235 of crater anomalies has been addressed by Lillis et al. (2010), who favour impact demag-
 236 netisation. Their models invoked a magnetic layer with uniform thickness but spatially
 237 varying magnetic properties that give rise to sizeable magnetic anomalies. By completely
 238 removing magnetisation within an inner circle, and allowing the magnetisation to ramp
 239 up within an annulus around this circle, they reduced the predicted anomalies. We change
 240 the thickness of the magnetised layer in a similar way, which should have the same ef-
 241 fect on the VIM as changing the magnetisation. Our models differ in that they do not
 242 consider any spatial variations in crustal magnetic properties.

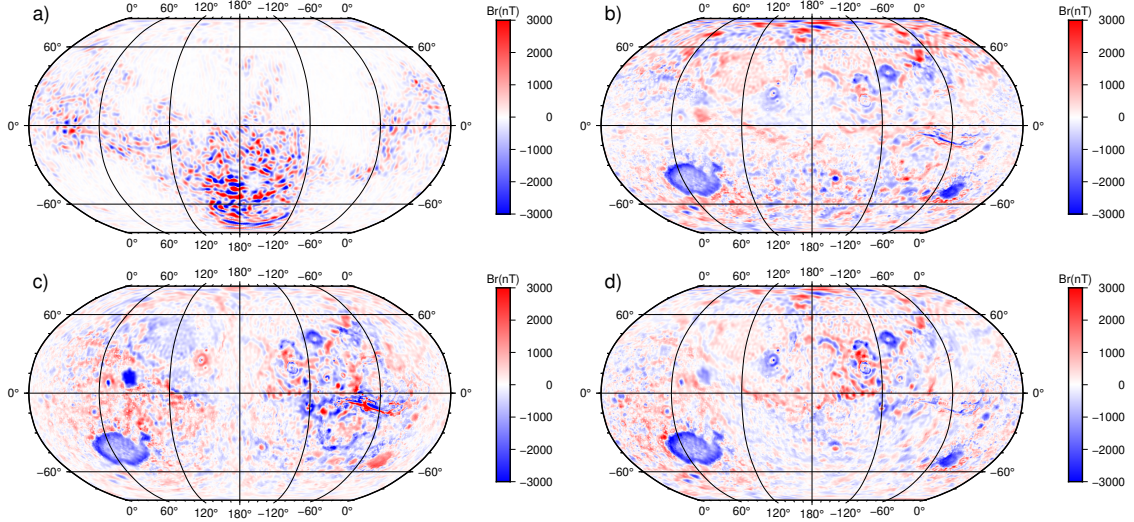


Figure 4. Radial component of the magnetic field at Mars surface. a: orbital model b: from VIM proportional to crustal thickness, magnetising field axial dipole ; c: equatorial dipole ($0^\circ\text{N}, 270^\circ\text{E}$); d: general paleopole ($34^\circ\text{N}, 202^\circ\text{E}$).

We removed the sharp step in VIM around Hellas by replacing the original thickness values in an annular region with radii 500 km and 2000 km, centered on the middle of the crater, with values derived by minimum curvature interpolation of the thickness outside the annulus as shown in Figure 5e. The magnetic anomaly is reduced (Figure 5c) but still substantial. We then returned to our central thesis, that a uniform VIM produces no magnetic anomaly, and interpolated across the entire crater, essentially filling it in. This does remove the magnetic anomaly (Figure 5d), but is hard to justify physically. One possible explanation is that the magnetic layer lies deep within the crust and any removal of shallow, non-magnetic material makes no difference. The problem is discussed further in Section 5. Results for the other 2 craters, Isidis and Argyre, are shown in Figures S6, S7.

VSH decomposition of the VIM for each of the 3 crustal thickness models shows that the \mathcal{E} component is reduced at the expense of \mathcal{I} and \mathcal{T} by interpolation but is increased by filling in. The RMS ratios $\mathcal{E}:\mathcal{I}:\mathcal{T}$ are 81:10:9, 81:10:9 and 85:7:8 respectively. This is to be expected as interpolation removes a small part of the shell whose magnetism is dominated by the \mathcal{E} part (but not enough to change the ratios at this resolution) while filling in adds material that is dominated by the \mathcal{E} part. Similar results and conclusions apply to the other craters, Isidis and Argyre: see the Supplementary Information Figures S6, S7.

5 Discussion and Conclusions

We have explored the use of VSH decomposition in evaluating possible magnetisation structures that could produce the observed Martian magnetic field. The ground measurement by InSight proves the existence of strong anomalies with wavelengths too short to be seen at satellite altitude. This requires strongly magnetised material at a relatively flat site that would not normally be thought as highly magnetic. Johnson et al. (2020) use Parker’s ideal body theory to estimate a lower bound on the magnetisation. They assume 40 km-thick magnetised layers starting at depths from 200 m down to 10 km and require magnetisations of $1.4\text{--}24\text{ Am}^{-1}$ or VIM $0.56\text{--}9.60 \times 10^5\text{ A}$, similar to the RMS of our \mathcal{I} part of $2.3 \times 10^5\text{ A}$. This is below the value required to explain the strong

Southern Hemisphere anomalies (Johnson et al., 2020). It is a lower bound so the true VIM must be larger. It also contains only the \mathcal{I} part of the VIM and there is no reason to believe the other invisible parts would be smaller: in fact there is every reason to suppose it is dominated by the \mathcal{E} part, as is the case on Earth (Masterton et al., 2012). If, as explored here, Mars' crust was magnetised globally by early cooling in a dynamo field, we expect the VIM to be 5–10 times bigger than this bound or our average estimate of the \mathcal{I} part.

Arkani-Hamed's inner shell of secondary magnetisation is interesting because, unlike the primary magnetisation, it is capable of producing an observable magnetic field. The VSH decomposition provides an exceptionally simple demonstration of this. While we have little new to report beyond that already published, VSH gives an elegant and simple formalism for exploring the primordial magnetising field.

A uniform magnetic layer magnetised by any dynamo field produces no magnetic anomalies: a spatially dependent VIM is needed. The obvious simple choice to explain the dichotomy, strong VIM in the Southern Hemisphere and weak in the Northern Hemisphere, produces anomalies around the equator rather than the required hemispheric difference. This applies for dipoles of most orientations and, because of the large uniform areas, is likely to apply for more complicated dynamo fields like hemispheric ones. We have shown how easy it is to produce a variety of magnetisations that fit the data exactly but this tells us nothing unless we can produce structures that are geologically plausible.

As a first step towards this goal we examined a magnetic layer that was uniformly magnetised but with variable thickness equal to the estimated crustal thickness from gravity and topography. This still produces a large \mathcal{E} part for any dynamo field, dominating the \mathcal{I} part that generates the anomalies. We had hoped this model might provide a starting point for further improvements to fit the data, but there are glaring disparities around the major impact craters, notably Hellas but also Isidis and Argyre. This casts doubt on the ideas that absence of magnetic anomalies around the craters is diagnostic of the absence of dynamo action when they were formed and removal of magnetised material by cratering.

In a new study Gong and Wiczorek (2021) have found the magnetisation in the southern highlands to be deeper than in the northern lowlands, which also means it is deeper at the sites of all 3 impact craters. If the upper 20 km of crust is unmagnetised around the craters then excavation or impact demagnetisation will have no effect and no magnetic anomaly will be produced. This seems to us the most likely explanation for the absence of any magnetic anomalies at these sites. Further work is needed on other craters to explore this idea.

Our long term goal is to develop a geologically plausible model for the magnetised layer at Mars' surface, focussed on specific anomalies. Our aim will be helped by future ground measurements from the Chinese rover Zhurong.

Acknowledgments

KZ is supported by the Macau Science and Technology Development Fund, grant No. 0005/2019/A1 and by the Pre-research Project on Civil Aerospace Technologies No. D020303 funded by China National Space Administration. SW is supported by NSFC project 41972237. YJ is supported by Macau Foundation. Our analysis made use of the codes `ctplanet` and `pyshtools` (Wiczorek & Meschede, 2018).

References

Andrews-Hanna, J. C., Zuber, M. T., & Banerdt, W. B. (2008). The borealis basin

- and the origin of the martian crustal dichotomy. *Nature*, *453*, 1212–1215. doi: 10.1038/nature07011
- Arkani-Hamed, J. (2003). Thermoremanent magnetisation of the Martian lithosphere. *J. Geophys. Res.*, *108*, 5114. doi: 10.1029/2003JE00204
- Arkani-Hamed, J. (2005). Magnetic crust of Mars. *J. Geophys. Res.*, *110*(E8), 20p. doi: 10.1029/2004JE002397
- Bloxham, J., & Gubbins, D. (1987). Thermal core-mantle interactions. *Nature*, *325*, 511–513.
- Bottke, W. F., & Andrews-Hanna, J. C. (2017). A post-accretionary lull in large impacts on early mars. *Nature Geoscience*, *10*, 344–348. doi: 10.1038/ngeo2937
- Frey, H., & Schultz, R. (1988). Large impact basins and the mega-impact origin for the crustal dichotomy on Mars. *Geophys. Res. Lett.*, *15*(3), 229–232.
- Gong, S., & Wieczorek, M. (2021). Depth of martian magnetization from localized power spectrum analysis. *J. of Geophys. Res.: Planets*, *126*(8), e2020JE006690. doi: <https://doi.org/10.1029/2020JE006690>
- Gubbins, D., Ivers, D., Masterton, S. M., & Winch, D. E. (2011). Analysis of lithospheric magnetisation in vector spherical harmonics. *Geophys. J. Int.*, *187*, 99–117.
- Hood, L. L., Harrison, K. P., Langlais, B., Lillis, R. J., Poulet, F., & Williams, D. A. (2010). Magnetic anomalies near Apollinaris Patera and the Medusae Fossae Formation in Lucus Planum, Mars. *ICARUS*, *208*(1), 118–131.
- Johnson, C. L., Mittelholz, A., Langlais, B., Russell, C. T., Ansan, V., Banfield, D., ... Banerdt, W. B. (2020). Crustal and time-varying magnetic fields at the InSight landing site on Mars. *Nature Geoscience*, *13*(3), 1–13.
- Ke, Y., & Solomatov, V. S. (2006). Early transient superplumes and the origin of the Martian crustal dichotomy. *J. Geophys. Res.*, *111*, E1001. doi: 10.1029/2005JE002631
- Langlais, B., Thébault, E., Houliez, A., Purucker, M. E., & Lillis, R. J. (2019). A New Model of the Crustal Magnetic Field of Mars Using MGS and MAVEN. *J. Geophys. Res.-Planets*, *124*(6), 1542–1569.
- Lewis, K. W., & Simons, F. J. (2012). Local spectral variability and the origin of the Martian crustal magnetic field. *Geophys. Res. Lett.*, *39*(18), 790. doi: 10.1029/2012GL052708
- Lillis, R. J., Dufek, J., Bleacher, J. E., & Manga, M. (2009). Demagnetization of crust by magmatic intrusion near the Arsia Mons volcano: Magnetic and thermal implications for the development of the Tharsis province, Mars. *J. Volcanology Geothermal Res.*, *185*(1-2), 123–138.
- Lillis, R. J., Frey, H. V., & Manga, M. (2008). Rapid decrease in Martian crustal magnetization in the Noachian era: Implications for the dynamo and climate of early Mars. *Geophys. Res. Lett.*, *35*(14). doi: 10.1029/2008GL034338
- Lillis, R. J., Purucker, M. E., Halekas, J. S., Louzada, K. L., Stewart-Mukhopadhyay, S. T., Manga, M., & Frey, H. V. (2010). Study of impact demagnetization at Mars using Monte Carlo modeling and multiple altitude data. *J. Geophys. Res. E: Planets*, *115*(7). doi: 10.1029/2009JE003556
- Marinova, M. M., Aharonson, O., & Asphaug, E. (2008). Mega-impact formation of the mars hemispheric dichotomy. *Nature*, *453*, 1216–1219. doi: 10.1038/nature07070
- Masterton, S., Gubbins, D., Mueller, D., Ivers, D., & Hemant, K. (2012). Forward modelling of oceanic lithospheric magnetisation. *Geophys. J. Int.*, *192*, 951–962.
- Milbury, C., & Schubert, G. (2010). Search for the global signature of the Martian dynamo. *J. of Geophys. Res.*, *115*(E10), 790–15.
- Mittelholz, A., Johnson, C. L., Feinberg, J. M., Langlais, B., & Phillips, R. J. (2020). Timing of the martian dynamo: New constraints for a core field 4.5 and 3.7 Ga ago. *Science Advances*, *6*(18), eaba0513.

- Morschhauser, A., Vervelidou, F., Thomas, P., Grott, M., Lesur, V., & Gilder, S. A. (2018). Mars' Crustal Magnetic Field. In *Magnetic fields in the solar system* (pp. 331–356). Springer International Publishing.
- Nimmo, F., & Gilmore, M. (2001). Constraints on the depth of magnetized crust on Mars from impact craters. *J. Geophys. Res.*, *106*, 12,315–12,323.
- Smrekar, S. E., Lognonné, P., Spohn, T., Banerdt, W. B., Breuer, D., Christensen, U., ... Wieczorek, M. (2018). Pre-mission insights on the interior of mars. *Space Science Reviews*, *215*, 3. doi: 10.1007/s11214-018-0563-9
- Solomon, S. C., Aharonson, O., Aurnou, J. M., Banerdt, W. B., Carr, M. H., Dombard, A. J., ... Zuber, M. T. (2005). New Perspectives on Ancient Mars. *Science*, *307*(5713), 1214–1220.
- Stanley, S., Elkins-Tanton, L., Zuber, M. T., & Parmentier, E. M. (2008). Mars' Paleomagnetic Field as the Result of a Single-Hemisphere Dynamo. *Science*, *321*(5897), 1822–1825.
- Thomas, P., Grott, M., Morschhauser, A., & Vervelidou, F. (2018). Paleopole reconstruction of martian magnetic field anomalies. *J. Geophys. Res.: Planets*, *123*(5), 1140–1155. doi: <https://doi.org/10.1002/2017JE005511>
- Voorhies, C. V. (2008). Thickness of the magnetic crust of Mars. *J. Geophys. Res.-Planets*, *113*(E04004). doi: 10.1029/2007JE002928
- Watters, T. R., McGovern, P. J., & Irwin III, R. P. (2007). Hemispheres Apart: The Crustal Dichotomy on Mars. *Ann. Rev. Earth Plan. Sci.*, *35*(1), 621–652.
- Wieczorek, M. A., Beuthe, M., Rivoldini, A., & Van Hoolst, T. (2019). Hydrostatic Interfaces in Bodies With Nonhydrostatic Lithospheres. *J. Geophys. Res.-Planets*, *124*(5), 1410–1432.
- Wieczorek, M. A., & Meschede, M. (2018). SHTools: Tools for Working with Spherical Harmonics. *Geochem., Geophys., Geosys.*, *19*, 2574–2592.
- Williams, S. E., & Gubbins, D. (2019). Origin of long-wavelength magnetic anomalies at subduction zones. *J. Geophys. Res.: Solid Earth*, *124*(9), 9457–9473. doi: <https://doi.org/10.1029/2019JB017479>
- Zhong, S., & Zuber, M. (2001). Degree-1 mantle convection and the crustal dichotomy on Mars. *Earth Planet. Sci. Lett.*, *189*, 75–84.

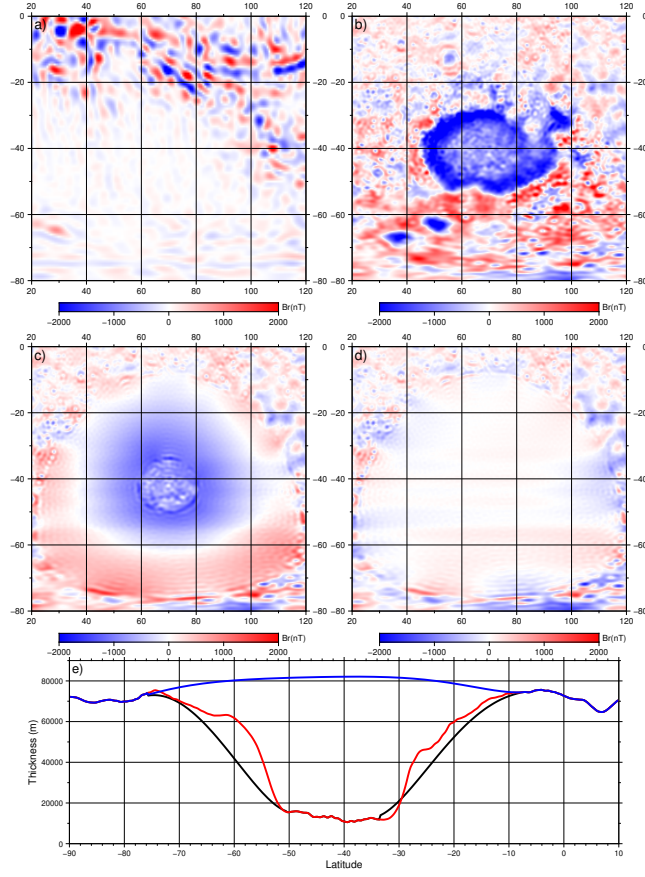


Figure 5. Close-up of the Hellas anomaly illustrating radial component of the magnetic field. a: orbital model (Langlais et al., 2019); b: original crustal thickness model; c: model with steep crater shoulders from (b) replaced with minimum curvature interpolation; d: crater removed altogether. e: North-South profile extracted along Longitude 70°E showing the crustal thickness profiles for the model cases shown in b (red), c (black) and d (blue) respectively.